Supplementary Information for

Red blood cell partitioning and segregation through vascular bifurcations in a model of sickle cell disease

May 29, 2025

1 Parameterization of Cell Shape

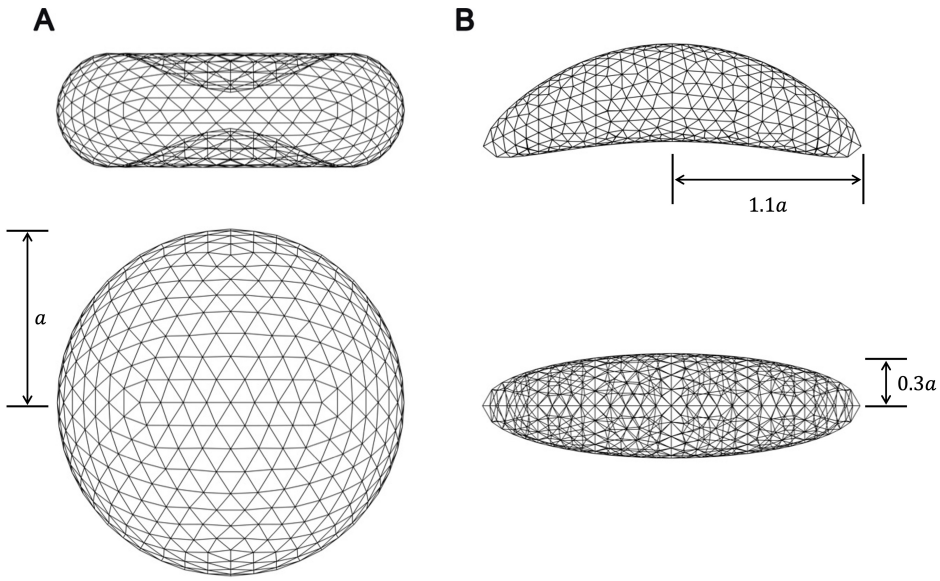

Fig. S1. The surface mesh for capsules of (A) biconcave-discoid normal RBC, and (B) sickle RBC. The radius of a normal RBC is $a = 4\mu m$.

Fig. S1 illustrates the rest shape of the cell models. A normal red blood cell (RBC) is represented as a flexible capsule with a biconcave discoidal rest shape [1, 2], characterized by the geometry:

$$y = \frac{a}{2}\sqrt{1-r^2}\left(C_0 + C_2 r^2 + C_4 r^4\right), \tag{1}$$

where $r^2 = x^2 + z^2 \leq 1$, with coefficients $C_0 = 0.2072$, $C_2 = 2.0026$, and $C_4 = -1.1228$. The parameter a represents the characteristic radius of the biconcave discoid, typically ranging from ~ 3.8 to $4.0\,\mu$m for human RBCs.

In contrast, an irreversibly sickled cell (ISC) exhibits a crescent shape, with a characteristic length slightly exceeding a [3, 4]. In this study, a sickle cell is modeled as a stiff capsule with a curved prolate spheroidal rest shape. This geometry is generated by first stretching a spherical capsule of radius a along its polar axis while compressing it along the equatorial plane, forming a slender prolate spheroid with polar radius $a_1 = 1.1a$ and equatorial radius $a_2 = 0.3a$. Then, a quadratic unidirectional displacement perpendicular to the polar axis is applied to the points, ultimately shaping the capsule into a curved prolate spheroid.

2 Cell Inflow and Outflow Boundary Conditions

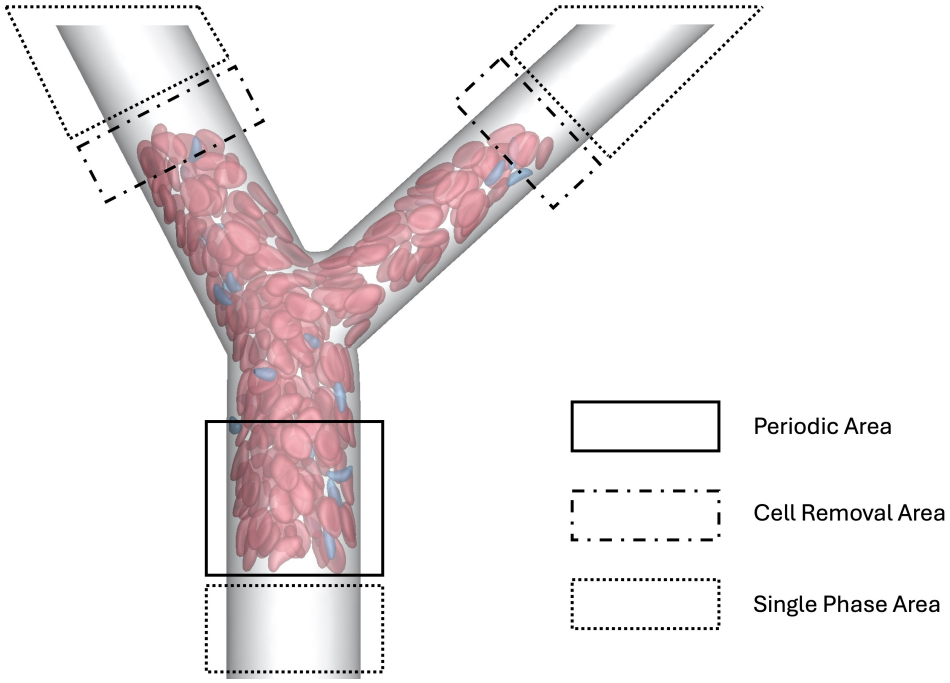

Fig. S2. Schematic diagram of the cell inflow and outflow boundary conditions used in this paper.

To investigate the effect of cell segregation at a vessel bifurcation, it is crucial that the distribution of cells and the cell-free layers are fully developed before reaching the core bifurcation region. To achieve this, our model employs an inflow and outflow boundary condition originally developed in [5], as illustrated in Figure **S2**. This approach is particularly advantageous for handling complex geometries that do not accommodate simple periodic boundary conditions. The implementation consists of three key components: (1) a periodic region, (2) single-phase flow regions near the vessel inlet and outlet, and (3) cell removal regions. The periodic region ensures continuous cell introduction, the single-phase flow regions stabilize the flow field, and the removal region maintains a dynamic equilibrium of cell numbers in the simulation. In addition, it is worth noting that since there are two types of cells considered in this work, the cell inflow and outflow boundary conditions need to be applied separately to each cell component.

In the periodic domain, the simulation is run long enough to achieve a statistically steady cell distribution, including sickle cell margination, without requiring flow through a pipe with a very spatially long entrance length. Once the statistically stationary distribution is established, cells that leave the periodic domain (and reenter the same domain in that simulation) are copied into the domain for the bifurcating vessel to generate a new cell that enters the upstream region domain. As a result, the number of cells within the periodic domain remains fixed, while the total number of cells in the bifurcation simulation is dynamic.

To ensure flow field stability, single-phase flow regions are placed near both the vessel inlet and outlet. Dirichlet velocity boundary conditions are applied in these regions to enforce Poiseuille flow profiles, enabling precise control over the relative flow rates in each sub-branch and adjustment of the volumetric partition ratio η_Q. Additionally, cells that enter the removal zone are continuously eliminated. This approach ensures that while the total number of cells in the simulation fluctuates, it eventually stabilizes within a small range. Furthermore, the sizes of the single-phase flow regions and the particle introduction/removal zones are designed to be sufficiently large to facilitate fully developed flow conditions, minimizing any unintended effects on the bifurcation region. To validate this design, we doubled the size of these regions and found no impact on the main conclusions drawn from our simulations.

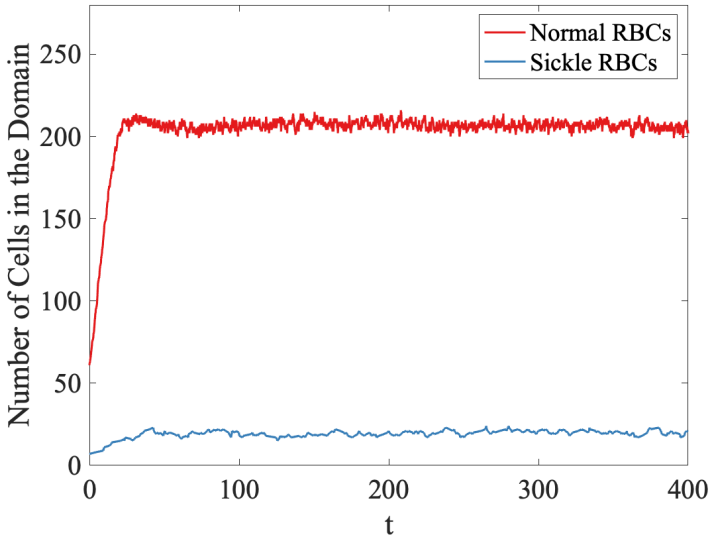

Fig. S3. Temporal evolution of the total number of (red) normal and (blue) sickle RBCs in central region of the computational domain. The simulation considers a SCD RBC suspension flowing through a geometrically symmetric bifurcated blood vessel with $\eta_Q = 0.5$.

To quantify the effect of bifurcated vessel boundary conditions on RBC flux fluctuations, we present the temporal variation of the total number of cells in Fig. **S3**. Upon the start of the simulation, the number of RBCs in the central region increases rapidly for about 50 strain units before reaching a statistically stationary state where the cell count stabilizes with minor fluctuations, indicating a dynamic balance between the influx and outflux of cells.

3 Confusion Matrix for the Normal and Sickle Cells Partition

The "prediction" statistic of 0.97 reported in the main text comes from the expression:

$$\text{Precision} = \frac{\text{True Positives}}{\text{True Positives} + \text{False Positives}},$$

where "positive" is defined as a cell that flows into the left channel of the bifurcation. Cell numbers were counted for 600 stain units. To further elucidate the classification performance, we have included confusion matrices for normal and sickle RBCs partitioning at $\eta_Q = 0.7$ in Tables S1 and S2.

Table S1. Confusion matrix for normal RBC partitioning at $\eta_Q = 0.7$.

Number of Normal RBCs	Predicted Positive	Predicted Negative
Actual Positive	3474	187
Actual Negative	98	1084

Table S2. Confusion matrix for sickle RBC partitioning at $\eta_Q = 0.7$.

Number of Sickle RBCs	Predicted Positive	Predicted Negative
Actual Positive	171	13
Actual Negative	8	87

References

[1] Evan Evans and Yuan-Cheng Fung. Improved measurements of the erythrocyte geometry. *Microvascular research*, 4(4):335–347, 1972.

[2] Kushal Sinha and Michael D Graham. Dynamics of a single red blood cell in simple shear flow. *Physical Review E*, 92(4):042710, 2015.

[3] HeeSu Byun, Timothy R Hillman, John M Higgins, Monica Diez-Silva, Zhangli Peng, Ming Dao, Ramachandra R Dasari, Subra Suresh, and YongKeun Park. Optical measurement of biomechanical properties of individual erythrocytes from a sickle cell patient. *Acta biomaterialia*, 8(11):4130–4138, 2012.

[4] JaeHwang Jung, Lucas E Matemba, KyeoReh Lee, Paul E Kazyoba, Jonghee Yoon, Julius J Massaga, Kyoohyun Kim, Dong-Jin Kim, and YongKeun Park. Optical characterization of red blood cells from individuals with sickle cell trait and disease in tanzania using quantitative phase imaging. *Scientific reports*, 6(1):31698, 2016.

[5] Zixiang L Liu, Jonathan R Clausen, Justin L Wagner, Kimberly S Butler, Dan S Bolintineanu, Jeremy B Lechman, Rekha R Rao, and Cyrus K Aidun. Heterogeneous partition of cellular blood-borne nanoparticles through microvascular bifurcations. *Physical Review E*, 102(1):013310, 2020.